AIAA JOURNAL
Vol. 34, No. 3, March 1996

Quantitative Measurements of Internal Circulation in Droplets Using Flow Tagging Velocimetry

Scott R. Harris,* Walter R. Lempert,† Leslie Hersh,‡ C. L. Burcham,§ Dudley A. Saville,¶ and Richard B. Miles**
Princeton University, Princeton, New Jersey 08544
and
Kyle Gee†† and Richard P. Haughland‡‡
Molecular Probes, Inc., Eugene, Oregon 97402

We demonstrate the use of the photoactivated nonintrusive tracking of molecular motion flow tagging technique to obtain quantitative velocity measurements in free falling water droplets and in electrohydrodynamic Taylor cones. A simple ray tracing procedure is outlined to remove the optical distortion caused by the droplet surface curvature. This correction is applied to free falling droplet images, and the vertical component of velocity is measured across the droplet. Maximum vertical velocities in the droplet are 15.9 ± 3.3 mm/s. Without ray tracing, the optical distortion is shown to cause errors in the sign of velocity as well as errors of over 100% in velocity magnitude. Preliminary velocity measurements in a Taylor cone are also presented. Centerline velocities in the Taylor cone are approximately 4 μ/s.

I. Introduction

TRANSPORT phenomena within droplets are known to play a role in a variety of processes, such as combustion and evaporation.[1] Nonetheless, the quantitative determination of the internal velocity field in a droplet presents a significant challenge to existing optical techniques. Johnson et al.[2] have demonstrated the use of a photochromic tracer for the quantitative measurement of the internal velocity field of 4–8 mm droplets during formation in a liquid-liquid spray column. The droplet fluid was Amsco petroleum solvent, and the outer, quiescent fluid was water. Reported velocities ranged up to 150 mm/s. Most other reported measurements have been quite qualitative in nature. For example, images of recirculation patterns have been obtained by time exposure of particles dispersed in large (order 1-cm) droplets, while falling in a viscous liquid, such as castor oil.[3] More recently, Winter[4] has reported evidence of internal circulation in 300–500 μ decane droplets free falling in air using a planar imaging technique based on oxygen quenching of naphthalene fluorescence. In this paper, we present two demonstrations of the use of the photoactivated noninstrusive tracking of molecular motion (PHANTOMM) flow tagging velocimetry technique to obtain quantitative velocity profiles in water droplets. The first example is an approximately 5-mm free falling water droplet with internal velocities in the range of ±16 mm/s. The second is an exceedingly slow electrohydrodynamic flow, known as a Taylor cone, with velocities on the order of 5 μ/s.

Flow tagging is a technique where a spatially continuous pattern is written into a flowfield by means of an optical resonance. The displacement of this pattern is subsequently tracked or interrogated by means of laser-induced fluorescence (LIF) imaging. The displacement that occurs during the elapsed time interval between the tagging and interrogation processes results in a measurement of velocity. In the gas phase, examples of flow tagging methods include Raman excitation plus laser-induced electronic fluorescence (RELIEF)[5] and multiphoton dissociation of water vapor, followed by (A, X) fluorescence from hydroxyl radical LIF.[6,7]

In the liquid phase, we have recently presented a new flow tagging approach based upon the use of caged dye photoactivated fluorophores (PAFs), which we have termed PHANTOMM.[8] Caged dye PAFs are nominally fluorescent dyes that are rendered nonfluorescent by the strategic attachment of a chemical caging group. The caging group is photolytically cleaved upon absorption of ultraviolet light, generally from a laser. After photolysis, the original fluorescent dye is recovered and can be tracked using laser sheet imaging techniques for times limited only by interspecies diffusion of the uncaged tracer molecules into the surrounding caged tracer solution. In essence, the technique is akin to ordinary dye visualization except that the dye is produced, in situ, in a specific pattern determined by the tagging laser geometry.[9]

The PHANTOMM technique is very similar in many respects to laser-induced photochemical anemometry (LIPA), which is based on the use of either photochromic or phosphorescent tracer materials. Photochromic materials exhibit a reversible change in reflectance when exposed to ultraviolet light, typically from either a nitrogen or excimer laser. Using backlighting, the temporal evolution of the initial reflectance pattern is tracked. Photochromic materials have been used almost exclusively in nonpolar solvents, although recently Yurechko and Ryazantsev[10] have reported measurements in water. Phosphorescent tracers are materials that absorb and re-emit light with a relatively long spontaneous radiative lifetime. Steir and Falco[11] have recently reported measurements in a simulated internal combustion engine using a water soluble tracer with a lifetime of between 0.30 and 0.80 ms. Recently LIPA has been reviewed by Falco and Nocera.[12]

II. Experimental Technique

Dextran carboxy fluorescein (commercially available from Molecular Probes, Inc.) was used as a tracer material in the work presented here. In the Taylor cone studies, the PAF used had a large dextran side chain resulting in a total molecular weight of 70,000. The large molecular weight limited the diffusion speed of the tracer, allowing a tagged line to be tracked for several minutes. In the free falling droplet work the molecular weight was 3000. The caging group is photolyzed upon the absorption of a single uv photon in

Presented as Paper 95-0168 at the AIAA 33rd Aerospace Sciences Meeting, Reno, NV, Jan. 9–12, 1995; received Feb. 16, 1995; revision received Aug. 7, 1995; accepted for publication Aug. 8, 1995.

*Graduate Student, Department of Mechanical and Aerospace Engineering. Student Member AIAA.
†Research Scientist, Department of Mechanical and Aerospace Engineering. Member AIAA.
‡Summer Researcher, Department of Mechanical and Aerospace Engineering; currently Undergraduate Student, University of Virginia, Charlottesville, VA 22904. Student Member AIAA.
§Graduate Student, Department of Chemical Engineering.
¶Professor, Department of Chemical Engineering.
**Professor, Department of Mechanical and Aerospace Engineering. Senior Member AIAA.
††Staff Scientist, 4849 Pitchford Avenue.
‡‡President, 4849 Pitchford Avenue.

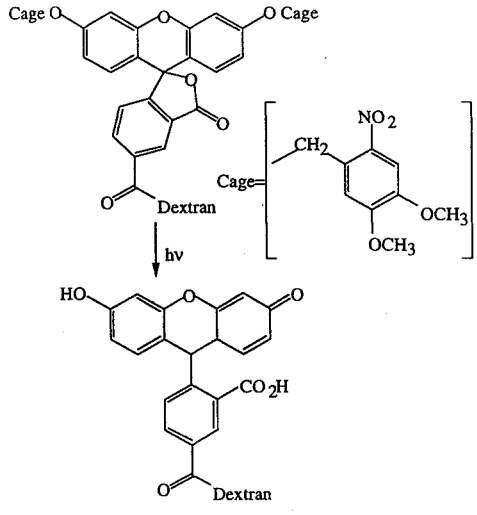

Fig. 1 Chemical structure of the caged and fluorescent forms of dextran carboxy fluorescein.

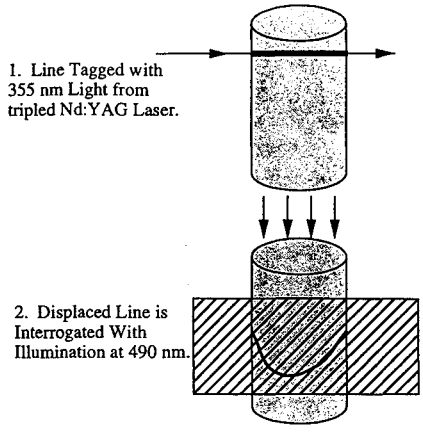

Fig. 2 Basic PHANTOMM flow tagging technique.

the region of 350 nm. Figure 1 shows the chemical structure of the caged and fluorescent forms of the dextran carboxy fluorescein PAF. The uncaged dye behaves essentially like ordinary fluorescein dye, strongly absorbing near 490 nm, with re-emission between 520 and 620 nm.

Figure 2 shows the basic optical configuration used in these experiments. The tagging is performed using the third harmonic of a Q-switched Nd:YAG laser at 355 nm. Single pulse energies between 2 and 20 mJ per pulse were used depending upon the experiment. Interrogation was performed using a flashlamp-pumped dye laser (Candela-LDFL-6) using LD490 dye in methanol with no intercavity line narrowing optics. The dye laser is capable of pulse outputs between 50 and 400 mJ, a pulse duration of approximately 2 μs, and a spectral bandwidth of approximately 1 nm.

III. Free Falling Droplets

Experimental Procedure

Figure 3 shows the experimental apparatus used in the free falling droplet studies. Water droplets approximately 5 mm in diameter are formed from a drawn glass tip that is gravity fed from a reservoir containing a 0.20 mg/L (6.7×10^{-8} M) solution of 3000 molecular weight dextran caged fluorescein. A helium neon laser beam passing below the tip exit serves as a trigger for the optical system. Single 1–2 mJ pulses of 355-nm light from a frequency tripled Nd:YAG laser are focused into the droplet using a 20-cm focal length plano convex lens. The tagging position is approximately 12.7 cm below the tip exit. The position of the tagging beam within the droplet is obtained by imaging the combined fluorescence and scatter from the tagging process onto a charge-coupled device (CCD) video camera (Sanyo model VDC-3800) with a 25-mm focal length lens. After a time delay varying between 16 and 29.5 ms the interrogation is performed

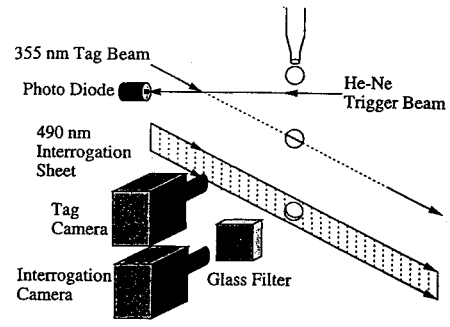

Fig. 3 Schematic drawing of apparatus used in the free falling droplet experiments.

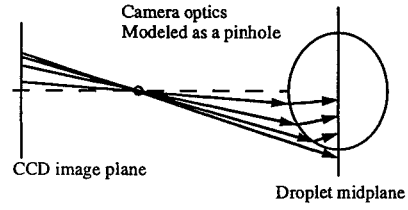

Fig. 4 Two-dimensional example of the ray tracing procedure used to remove the optical distortion produced by viewing tagged lines through the front surface of a water droplet. Each pixel on the CCD is traced back to its origin on the droplet mid plane. Actual computations are done in three dimensions.

using a single 10–20 mJ pulse from the dye laser, formed into an approximately 1-cm-high by 300-μ-thick sheet. The fluorescence of the tagged line is imaged with a second CCD video camera (Cohu model 4810) using a 50-mm focal length lens. The magnification of both imaging systems is approximately 0.8. A simple colored glass filter (OG-515) is used to block the elastic scattering from the droplet and transmit the fluorescence of the tagged line. Both the tag and interrogation images are captured with a freeze frame unit and stored on VHS videotape for later postprocessing with a computer frame grabbing system.

The droplet surface itself acts as a lens, introducing significant optical distortion. Zhang and Melton[13] have developed a technique that removes both the geometrical and intensity distortion caused by spherical droplets. In this work, only the geometric distortion was removed. A simple ray tracing procedure was used to trace the ray falling on each element of the CCD back to its source in the droplet. Figure 4 shows a schematic of this process. In the ray tracing procedure, the imaging system is modeled as a pinhole. The location of this pinhole, together with the location of each pixel on the CCD, defines a unique ray along which the light striking the pixel in question must have come. This ray is projected backwards until it either strikes a plane passing through the center of the droplet or the droplet surface, which is modeled as an ellipsoid. If the ray strikes the ellipsoid first, it is refracted according to Snell's law and is projected again until it strikes the droplet midplane. Once the ray reaches the droplet midplane, the intensity value at the origin of the ray is transferred to its new location on the droplet midplane.

The ray tracing program takes as its parameters the focal length of the imaging system, the magnification of the imaging system, the major and minor axes of an axisymmetric ellipsoid representing the surface of the drop, and two coordinates describing the center of this ellipsoid. These parameters related to the size and position of the droplet were found by thresholding the interrogation image to a value halfway between the average intensity values inside and outside the drop. Any pixel with a grayscale intensity value less/greater than this critical value was set to a value of zero/one, respectively. An ellipse was then fit to the resulting binary image. The parameters of this ellipse were taken to be the size of the droplet and input to the ray tracing program. In addition, the ellipse bounding the drop was determined by visual estimation, and it was found that these two approaches give line positions after ray tracing that generally do not differ by more than 2 pixels (7.0×10^{-2} mm). Because the background fluorescence in the tagging images was not as uniform

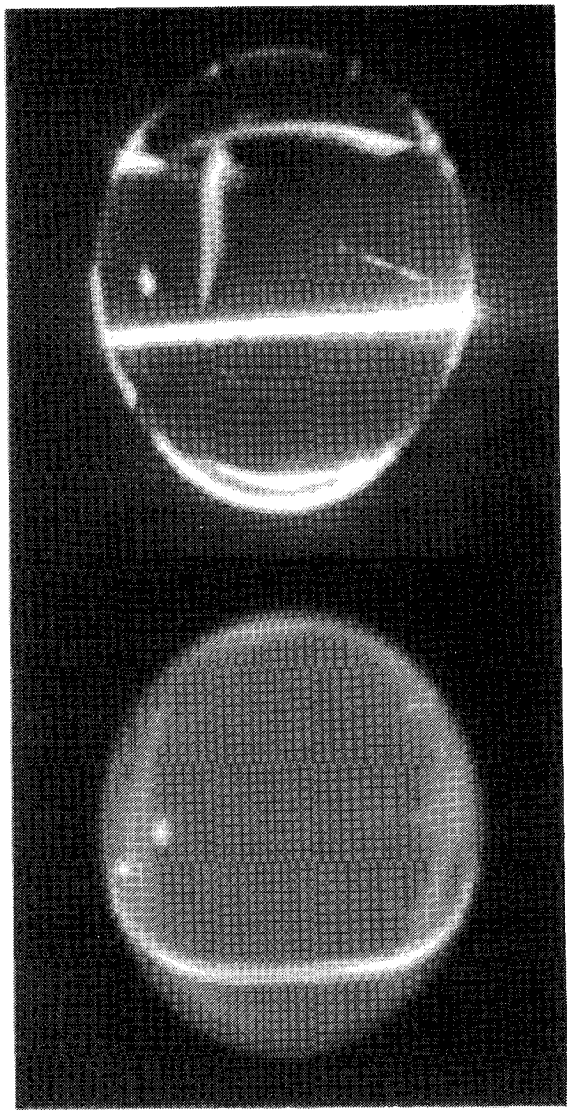

Fig. 5 Images of droplet with tagged line (top) and interrogated line 29.5 ms later (bottom).

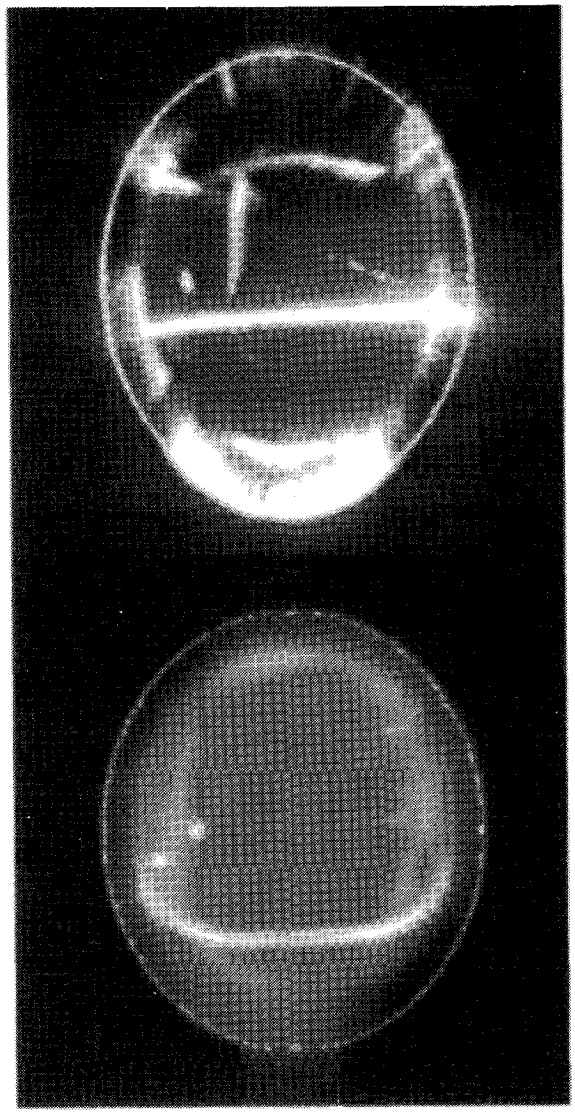

Fig. 6 Images of tagged (top) and interrogated lines (bottom) with optical distortion removed.

as that in the interrogation images, the boundary of the droplet was not well defined, and it was necessary to estimate visually the major and minor axes of the bounding ellipsoid, as well as its center.

After ray tracing, the resulting image is masked by hand to leave only the region immediately surrounding the tagged line. The intensity as a function of vertical position on the image is least-squares fit to a Gaussian with a linearly varying background to locate the line center for each column in the picture. The linearly varying background was found to give a better representation of the raw data. Typical σ values for the statistical uncertainties in the line centers determined by these fits range from 0.02 to 0.1 pixels (7.0×10^{-4}–3.5×10^{-3} mm). Finally, the resulting displacement data, together with the time between tag and interrogation, are used to compute the component of velocity perpendicular to the original tagged line.

Results

Figure 5 shows a pair of representative tag and interrogation images that have been corrected for nonunity aspect ratio of the CCD and frame-grabbing system. The time delay between tag and interrogation is 29.5 ms. In Fig. 5 the strong scattering from the tagging beam resulted in a saturated tagging image. This can be avoided through the use of a neutral density filter. Figure 6 shows the same droplets as in Fig. 5 above after applying the ray tracing correction.

Figure 7 shows representative interrogated line positions that resulted from performing the ray tracing procedure with several

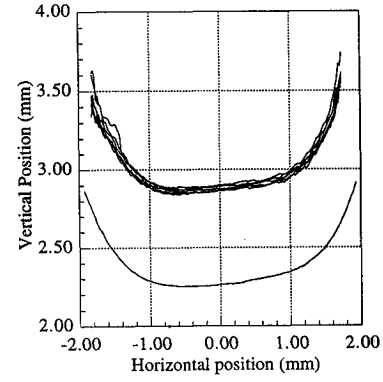

Fig. 7 Interrogated line positions calculated with (top) and without (bottom) ray tracing correction.

different sets of droplet shape parameters, all of which differed by approximately their experimental uncertainty. For reference, the non-ray-traced result is also shown. These variations in the ray traced line positions correspond to the 2 pixel uncertainty in line position mentioned earlier. Figure 8 shows the position of the tagged line with and without the ray tracing correction, as well as linear fits to these data.

From Figs. 5 and 6, it is clear that the droplet curvature distorts the view of its interior by stretching the images in the radial direction. Furthermore, a region around the edge of the droplet approximately

Table 1 Contributions of uncertainty in line position, image size calibration, and time delay to overall experimental uncertainty

	$\left(\frac{k}{\Delta t}\right)^2\left(\sigma_{x_1}^2+\sigma_{x_2}^2\right)$	$\left[\frac{(x_2-x_1)}{\Delta t}\right]^2\sigma_k^2$	$\left[\frac{(x_2-x_1)}{\Delta t^2}\right]^2\sigma_{\Delta t}^2$	σ_v
With ray tracing	11.21 mm^2/s^2	3.75×10^{-2} mm^2/s^2	2.38×10^{-4}mm^2/s^2	3.35 mm/s
Without ray tracing	2.80×10^{-2} mm^2/s^2	3.75×10^{-2} mm^2/s^2	2.38×10^{-4}mm^2/s^2	0.256 mm/s

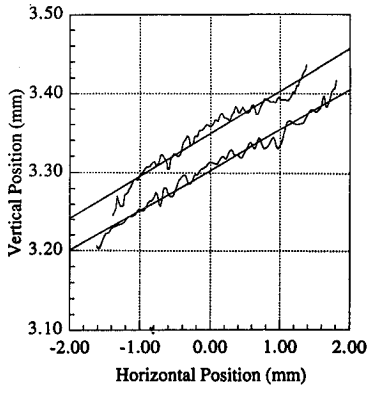

Fig. 8 Tagged line positions calculated with (top) and without (bottom) ray tracing correction.

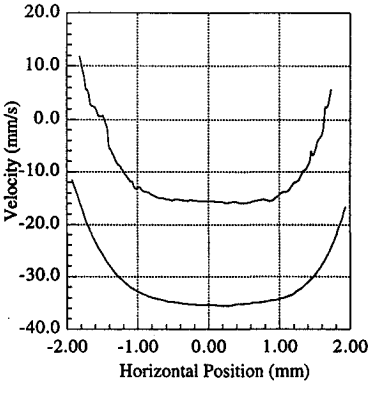

Fig. 9 Velocity data calculated with (top) and (bottom) ray tracing correction.

0.3 mm wide is obscured, and data from this region are unavailable. Figure 9 shows velocity data for the same drop calculated with and without employing the ray tracing correction. Without ray tracing, the distorted images give the unphysical result that the velocities in the droplet are all negative (downward). The results after ray tracing, however, show the velocities becoming positive near the sides, consistent with internal circulation. The maximum velocity inside the droplet, calculated with the ray tracing correction was −15.9 mm/s. Without this correction, the maximum calculated velocity in the droplet was −35.5 mm/s.

Errors

The equation used to calculate velocities is

$$v = k(x_2 - x_1)/\Delta t \tag{1}$$

where k is the measured calibration from pixels (in the image plane), to millimeters (in the object plane). Performing a standard error propagation, we obtain the result that

$$\sigma_v^2 = \left(\frac{k}{\Delta t}\right)^2\left(\sigma_{x_1}^2+\sigma_{x_2}^2\right)+\left[\frac{(x_2-x_1)}{\Delta t}\right]^2\sigma_k^2 + \left[\frac{(x_2-x_1)}{\Delta t^2}\right]^2\sigma_{\Delta t}^2 \tag{2}$$

The first, second, and third terms correspond to uncertainties in the line position, image size calibration, and time delay between tag and interrogation, respectively. Table 1 shows the contributions to the error from each term, for measurements with and without ray tracing. It is clear that the dominant error in this procedure results from the large (2 pixels) uncertainty in line position produced by the ray tracing procedure. If the droplet surface could be more accurately defined, or if ray tracing were not necessary, the total error would be substantially reduced and errors due to line location uncertainty would be approximately equal to those introduced by uncertainties in camera calibration. With ray tracing, the error in velocity is 3.35 mm/s or 21% of the maximum measured velocity in the droplet. Without ray tracing, the error in velocity is only 0.256 mm/s or 1.6% of the maximum measured velocity.

In addition to the preceding errors, there is also systematic uncertainty inherent in the assumption that the velocity is accurately described by Eq. (1). We can express the tag location in terms of the interrogated position via a Taylor series:

$$x_{\text{tag}} = x_{\text{int}} - \left.\frac{dx}{dt}\right|_{x_{\text{int}}}\Delta t + \left.\frac{d^2x}{dt^2}\right|_{x_{\text{int}}}\frac{\Delta t^2}{2} - \mathcal{O}(\Delta t^3) \tag{3}$$

Rearranging, we can write that

$$v = \left.\frac{dx}{dt}\right|_{x_{\text{int}}} = \frac{x_{\text{int}}-x_{\text{tag}}}{\Delta t} + \left.\frac{dv}{dt}\right|_{x_{\text{int}}}\frac{\Delta t}{2} - \mathcal{O}(\Delta t^2) \tag{4}$$

We take

$$\left.\frac{dv}{dt}\right|_{x_{\text{int}}}\frac{\Delta t}{2}$$

to be an estimate of the error. Identifying the Lagrangian derivative

$$\left.\frac{dv}{dt}\right|_{x_{\text{int}}}$$

as the Eulerian total derivative

$$\frac{Dv}{Dt} = \frac{\partial v}{\partial t} + v\cdot\nabla v$$

allows an analysis of the systematic uncertainty. Assuming that the second term in the Eulerian derivative is dominant and that the maximum gradient of velocity in the droplet is of order $V_{\max}/R$ implies that the maximum uncertainty in the velocity measurement is approximately $\Delta t V_{\max}^2/2R$, which is 1.8 mm/s or 12% of the maximum velocity in the droplet. The systematic uncertainty can be reduced either by reducing the time delay between tag and interrogation or by interrogating multiple times and using a higher order stencil to approximate the velocity.

IV. Taylor Cone Studies

Electrohydrodynamic fluid motion is driven by an externally applied electric field. The electric field creates motion by acting as a surface stress at the interface of a two-phase system. A charge is induced at the interface, due to the difference in dielectric constant and conductivity of the two phases. As a result of this induced charge, the interface deforms under the influence of the external field. At the interface, the tangential electrical stress is balanced by viscous forces, and the normal electrical stress is balanced by surface tension and pressure differences between the two phases. The viscous forces result in velocity gradients in the two phases.

Taylor cones are one example of electrohydrodynamic flows.[14,15] A Taylor cone is formed by placing a drop of one fluid on an electrode. An electric field is created by placing another electrode above the droplet and applying a potential difference. As the electric field is increased, the drop deforms into a quasi-steady-state shape in the form of a cone emitting a jet of fluid from its tip.

Traditionally, flow visualizations in these systems have been obtained using small tracer particles such as talc or alumina.[16,17] These tracers can become charged and give biased information about the flowfield.

Experimental Procedure

Figure 10 shows a schematic illustration of the experimental apparatus used to study Taylor cones. A pair of electrodes immersed in high-viscosity silicone oil are attached to a high-voltage power supply to provide the external field. A small sessile droplet is produced by injecting a 10 mg/L (1.4×10^{-7} M) solution of 70,000 MW dextran carboxy fluorescein through a small hole in the bottom electrode. A 5-mm-diameter nylon ring centered around this hole prevents the droplet from wetting the entire electrode. As the electric field is increased, the droplet deforms into a Taylor cone. The uv light from the Nd:YAG laser is focused so that the beam waist is centered at the axis of the cone. The diameter of the beam passing through the cone is approximately 50 μ. The beam can be raised or lowered so that the entire cone can be examined.

Results

Because the Taylor cone is surrounded by silicone oil, with an index of refraction of approximately 1.5, there is some degree of index matching and no correction was applied to remove the distortion caused by viewing the tagged lines through the conical water/silicone oil interface. Figure 11 shows a droplet resting on the bottom electrode and the Taylor cone that results when a field of 2.07 kV/cm is applied. Figure 12 shows a representative sequence of images showing the evolution of a single line tagged near the top of the cone. The images correspond to time delays of 0.00, 17.92, 44.43, and 78.63 s, respectively, clockwise from upper left.

Preliminary estimation of line locations were obtained by assuming the highest grayscale intensity value to correspond to the location

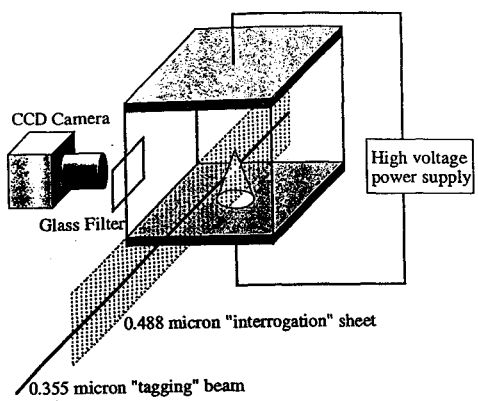

Fig. 10 Schematic illustration of the experimental apparatus used to study Taylor cones.

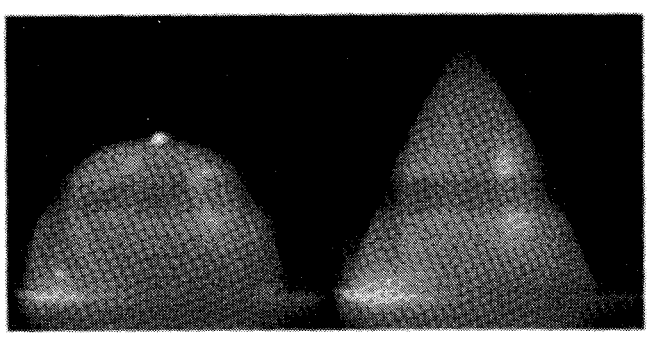

Fig. 11 Sessile drop on bottom electrode with no applied field (left) and Taylor cone 206 s later. Field strength is 2.07 kV/cm.

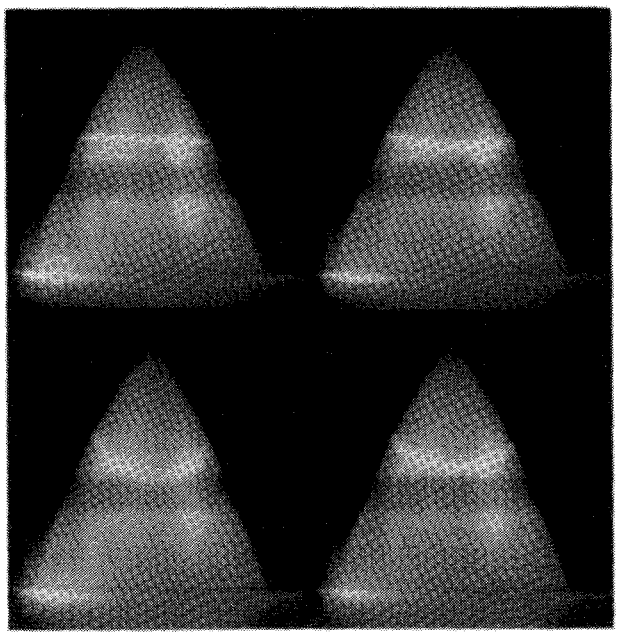

Fig. 12 Sequence of PHANTOMM images in a Taylor cone: t = 0.00, 17.92, 44.43, and 78.63 s (clockwise from upper left).

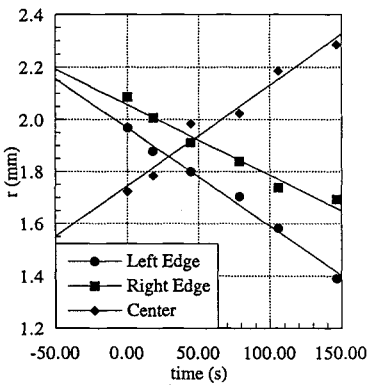

Fig. 13 Position of tagged line in Fig. 12 with linear fits; r is the radial distance from the tip of the cone to the tagged line.

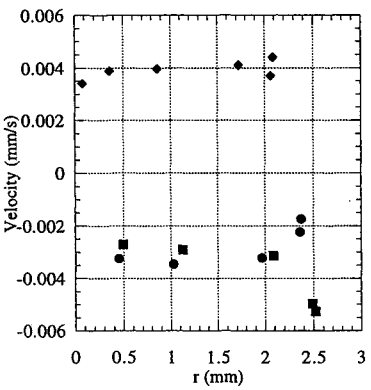

Fig. 14 Radial velocities measured in Taylor cone. Legend is the same as in Fig. 13.

of the line center. Because the lines were at most 4 pixels wide, this introduces an error in line location of up to 2 pixels (0.02 mm). The displacement of the tagged line and the velocities inside the cone were calculated for the cone axis and along the edges. Figure 13 shows the position of the tagged line in Fig. 12 as a function of time for the left and right edges, as well as on the axis of the cone. Straight lines were fit to these data and the slope of the fit was taken as a measure of velocity. Additional lines were tagged in the cone at other locations and the same procedure was repeated. Figure 14 shows the velocities calculated using this method.

V. Conclusions

We have demonstrated a new diagnostic technique capable of obtaining quantitative internal velocity data in water droplets. A simple procedure for removing geometrical distortion from the droplet itself has been developed. This distortion, if not removed, can result in errors in both the magnitude and sign of the velocity.

Acknowledgments

This work was sponsored by the National Science Foundation, Robert Powell, technical monitor, and the NASA Microgravity Science and Applications Program. The first author received support from the U.S. Air Force Palace Knight Program. The authors would like to thank Philip Felton for several stimulating discussions and Philip Howard for providing technical assistance.

References

[1]Winter, M., and Melton, L. A., "Measurement of Internal Circulation in Droplets Using Laser-Induced Fluorescence," *Applied Optics*, Vol. 29, No. 31, 1990, pp. 4574–4577.

[2]Johnson, G. R., Marschall, E., and Esdorn, J. H., "Improved Flow Visualization Technique for Quantitative Velocity Measurement in Small Test Volumes," *Review of Scientific Instruments*, Vol. 56, No. 2, 1985, p. 264.

[3]Clift, R., Grace, J. R., and Weber, M. E., *Bubbles, Drops, and Particles*, Academic, New York, 1978.

[4]Winter, M., "Droplet Slicing Measurements of Internal Circulation," AIAA Paper 93-0900, Jan. 1993.

[5]Miles, R. B., Connors, J. J., Markovitz, E. C., Howard, P. J., and Roth, G. J., "Instantaneous Profiles and Turbulence Statistics of Supersonic Free Shear Layers by Raman Excitation Plus Laser-Induced Electronic Fluorescence (RELIEF) Velocity Tagging of Oxygen," *Experiments in Fluids*, Vol. 8, No. 1/2, 1989, pp. 17–24.

[6]Boedeker, L. R., "Velocity Measurement with Enhanced OH Flow Tagging," *Optics Letters*, Vol. 14, No. 10, 1989, pp. 473–475.

[7]Chen, T., Schommer, D., and Gross, L., AIAA Paper 92-0008, Jan. 1992.

[8]Lempert, W. R., Magee, K., Gee, K. R., and Haugland, R. P., "Flow Tagging Velocimetry in Incompressible Flow Using PHoto Activated Nonintrusive Tracking Of Molecular Motion (PHANTOMM)," *Experiments in Fluids*, Vol. 18, No. 4, 1995, pp. 249–257.

[9]Dahm, W. J. A., and Dimotakis, P. E., "Mixing at Large Schmidt Number in the Self-Similar Far Field of Turbulent Jets," *Journal of Fluid Mechanics*, Vol. 217, Aug. 1990, pp. 299–330.

[10]Yurechko, V. N., and Ryazantsev, Y. S., "Fluid Motion Investigation by the Photochromic Flow Visualization Technique," *Experimental Thermal and Fluid Science*, Vol. 4, No. 3, 1991, pp. 273–288.

[11]Steir, B., and Falco, R. E., "New Developments in Laser-Induced Photochemical Anemometry (LIPA)," *Proceedings of SPIE Symposium on Optical Diagnostics in Fluid and Thermal Flow* (San Diego, CA), SPIE, Bellingham, WA, 1993.

[12]Falco, R. E., and Nocera, D., "Quantitative Multi-Point Measurements and Visualization of Dense Liquid-Solid Flows Using Laser-Induced Photochemical Anemometry (LIPA)," *Particulate Two-Phase Flow*, edited by M. C. Roco, Butterworth–Heinemann, Boston, 1993, pp. 59–126.

[13]Zhang, J., and Melton, L. A., "Numerical Simulations and Restorations of Laser Droplet-Slicing Images," *Applied Optics*, Vol. 33, No. 2, 1994, pp. 192–200.

[14]Vizka, O., and Saville, D. A., "The Electrodynamic Deformation of Drops Suspended in Liquids in Steady and Oscillatory Electric Fields," *Journal of Fluid Mechanics*, Vol. 239, June 1992, pp. 1–21.

[15]Wohlhuter, F. K., and Basaran, O. A., "Shapes and Stability of Pendant and Sessile Dielectric Drops in an Electric Field," *Journal of Fluid Mechanics*, Vol. 235, Feb. 1992, pp. 481–510.

[16]Melcher, J. R., and Taylor, G. I., "Electrohydrodynamics: A Review of the Role of Interfacial Shear Stresses," *Annual Review of Fluid Mechanics*, Vol. 1, 1969, pp. 11–146.

[17]Hayati, I., "Eddies Inside a Liquid Cone Stressed by Interfacial Electrical Shear," *Colloids and Surfaces*, Vol. 65, No. 1, 1992, pp. 77–84.